Engineering Geology xxx (2008) xxx–xxx

Contents lists available at ScienceDirect

Engineering Geology

journal homepage: www.elsevier.com/locate/enggeo

Simulation of Tsaoling landslide, Taiwan, based on Saint Venant equations over general topography

C.Y. Kuo [a,*], Y.C. Tai [b], F. Bouchut [c], A. Mangeney [d], M. Pelanti [c], R.F. Chen [e], K.J. Chang [f]

[a] Division of Mechanics, Research Center for Applied Sciences, Academia Sinica, Taiwan
[b] Department of Civil Engineering, National Chi-Nan University, Nantou, Taiwan
[c] Département de Mathématique et Applications, École Normale Supérieure et CNRS, Paris, France
[d] Institut de Physique de Globe de Paris, University Paris-Diderot, France
[e] Institute of Earth Sciences, Academia Sinica, Taiwan
[f] Department of Civil Engineering, National Taipei University of Technology, Taiwan

ARTICLE INFO

Article history:
Received 22 April 2008
Received in revised form 30 September 2008
Accepted 4 October 2008
Available online xxxx

Keywords:
Arbitrary topography
Chi-Chi earthquake
Earthquake triggered landslide
Rock-and-soil avalanche
Tsaoling geology
Tsaoling landslide

ABSTRACT

The 1999 Chi-Chi earthquake triggered the catastrophic Tsaoling landslide in Taiwan. The geomorphological change measured from the data of the 1989 and 2000 aerial photos reveals that the scar and deposit volumes are about 0.126 km^3 and 0.15 km^3 respectively. The debris material ran over a distance of 1.6 km with 500 m descent in elevation. In this paper, we use the continuum model of hydraulic flow, SHALTOP^{2D}, based on the equations of Bouchut and Westdickenberg to simulate numerically the landslide dynamics. When the mass is moving, the flow is assumed hydrostatic with a basal Coulomb friction. The best fit is obtained using the basal friction angle equal to 6°, the only parameter of the simulation, uniformly applied in the calculation domain. The landslide front reaches the Chinshui river valley, the foothill of the slope, within only about 25 s after initiation and the motion settles in about 113 s. The maximum speed is estimated 75 m/s. The spreading of the deposit agrees well with the field measurement.

1. Introduction

Taiwan island is located between the Philippine Sea plate and the Eurasian plate, with the two opposite-verging subduction systems of the Ryukyu arc-trench and Luzon arcs. Therefore, Taiwan is one of the regions on Earth with the highest seismic activity. On the 21st of September, 1999, Chi-Chi earth-quake (M_L=7.3) struck the central Taiwan at 01:47 local time. This earthquake was the most destructive one in the last century in Taiwan and caused more than 2450 fatalities and wide spread damage. It also triggered more than 9000 landslides over 128 km^2 in the central mountain area of the island (Liao, 2000).

Tsaoling landslide is one of the most catastrophic landslides (Hung, 2000). More than 0.126 km^3 of material ran over a distance of 1.6 km with 500 m descent in elevation (Chen et al., 2006b). The deposit volume increased to about 0.150 km^3 due to rupture of the sliding mass at motion. The deposit caused the fourth formation of the block dam of Chin-Sui River at the foothill of the slope in the local history (Chen et al., 2006b). 39 people were killed and 7 survived in a van after gliding with the landslide.

Field investigations and reported data reveal that the Tsaoling landslide is a typical rock avalanche in many aspects (Hung et al., 2002). The evidence includes chaotic distribution of large rock blocks, flow morphology and internal structure and relative thinness in comparison to large aerial extent, high porosity, angularity of fragments, and the lobate forms etc. Although extensive report documented the geomorphological evolution, rock material properties, and risk analysis (Hung et al., 2002; Chen et al., 2003, 2005), there are yet no conclusive reports on the duration of the landslide, velocity and impact response of the sliding mass into the deposit valley.

An early attempt using the discrete element method (DEM), based on the commercial PFC 3D code, were made by Tang and Hu (2004). However, the concluding almost-zero fiction angle between particles may not be able to reflect the event realistically. Alternative estimation is still being sought which can provide valuable information for future plans, e.g. conservation, hazard prevention etc., of this site.

Besides the DEM simulation, the continuum models have gained significant progress in the past few decades. Savage and Hutter (1989) assumed that the materials in avalanches follow the Mohr–Coulomb constitutive law and the Coulomb friction law at the basal surface, and derived a one-dimensional model. Savage and Hutter (1991), Gray et al. (1999), and Pudasaini and Hutter (2003) extended the theory to two-dimensional models and demonstrated good agreements with the laboratory measurements, see Pudasaini and Hutter (2007). The Mohr–Coulomb constitutive relation is rooted from the classical soil mechanics and since then is widely adopted in various versions of the

* Corresponding author.
E-mail address: cykuo06@gate.sinica.edu.tw (C.Y. Kuo).

0013-7952/$ – see front matter © 2008 Elsevier B.V. All rights reserved.
doi:10.1016/j.enggeo.2008.10.003

avalanche models. Iverson and Denlinger (2001) and Denlinger and Iverson (2001) combined the Mohr–Coulomb constituent with fluid rheology and proposed a Coulomb mixture model. Their theory is verified with measurements of laboratory tests using plane chutes. Subsequently, McDougall and Hungr (2004), adopting the Coulomb mixture rheology and including the erosion mechanism at the base, found good agreements between the simulation and the field measurement of a real event, the Frank slide, Canada, 1903. Effects of the erosion mechanism and the fluid rheology on the avalanche runouts were numerically investigated by Chen et al. (2006a) and they are shown of importance when applied to shallow landslides, e.g. the Bianzone debris flows, Italy, 2000. The above works all demonstrate the capability of the continuum models to reproduce the rapid motion of flows densely packed with discrete granules/particles.

The purpose of this paper is to use a recently developed continuum model to simulate the Tsaoling landslide and to provide the kinematic characteristics of interest of the landslide. However, there remain heuristic assumptions in the aforementioned models with the Mohr–Coulomb constituent: namely, the hypothesis that the principal axes of the stress are in parallel to the flow direction and some hypotheses for the determination of the passive/active stress state of the flow, which vary according to the different model proposals, e.g. Gray et al. (1999), Iverson and Denlinger (2001) and McDougall and Hungr (2004). While these assumptions are appropriate for the well-defined debris flow chute channels in laboratory experiments and the reported applications, they may yield undesired and unknown effects in the present Tsaoling slide. This is because of the river valley at the foothill of the sliding slope, which provides an impingement zone and splits the avalanche flow into two separate directions, cf. Section 2. It is expected that sophisticated flow interactions can take place in the river valley and can break the above two assumptions. Hence, at this stage, we adopt a hydraulic model with Coulomb basal friction to avoid the complications.

In the hydraulic model, the avalanche flow is assumed incompressible, thin and with a uniform velocity profile across the depth but with a basal Coulomb friction. Because the viscosity does not play a role in the model, the material constituent of the flow is sometime referred to as an Eulerian fluid. This approach has been widely applied in snow avalanches in the early Russia literature, see page 121, Pudasaini and Hutter (2007). Gray et al. (2003) show that, even under these aggressive simplifications, the model can accurately predict the outstanding physical phenomena, e.g. granular shock waves, dead zones etc., observed in debris avalanches. In order to account for the real topography in the present application, we adopt the flow model based on the equations of Bouchut and Westdickenberg (2004) and developed through a long term collaboration between DMA, ENS (F. Bouchut) and IPGP (A. Mangeney). The model equations are derived for arbitrary topography in a way that is convenient for many practical applications, such as incorporating GIS data without the need of performing a coordinate transformation. Using this hydrostatic model or the flow law proposed by Pouliquen and Forterre (2002), Mangeney-Castelnau et al. (2005), Mangeney et al. (2007), Pirulli and Mangeney (2008) and Lucas and Mangeney (2007) show that laboratory experiments as well as real flows on Earth and on Mars can be reproduced with a good accuracy. With the simple Coulomb basal friction law, the only parameter of investigation from the real measurements is the friction angle. On the justifications made therein, the simulation is expected to be able to provide many informative details of the response and flow characteristics of the landslide.

2. Geology and history of Tsaoling area

The Tsaoling area is located in the northeast of Yunlin County, the foothill of the central mountain region, Fig. 1, near the southern end of the Chelunpu fault. The earthquake caused a surface rupture, more than 90 km from Miaoli to Chiayi County, along the Chelunpu fault. Vertical offsets on average from 2 m to 4 m from the south to the north of the fault and the widest horizontal offsets up to 10 m are observed (Lin et al., 2001b).

The study area is shown in Fig. 2. Chinshui River flows along the base of the dip slope, cuts into the toe of the slope and causes the bedding of the foothill of the slope exposed to the surface. The elevation of the slope ranges from 500 m to 1200 m above the sea

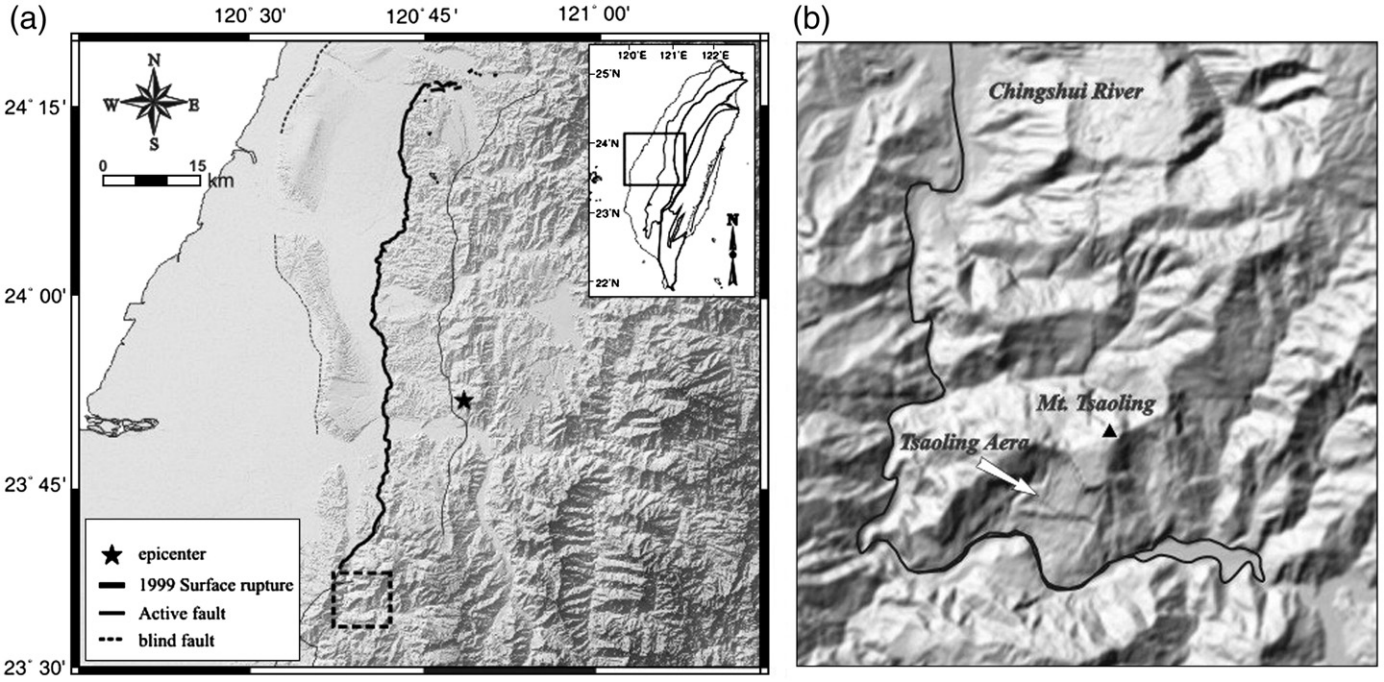

Fig. 1. (a) Central-west of Taiwan and the surface rupture of the Chelungpu Fault and the 1999 Chi-Chi earthquake epicenter. (b) Shaded topographic map of the Tsaoling region before the earthquake, on 1989 40×40 m DEM.

Please cite this article as: Kuo, C.Y., et al., Simulation of Tsaoling landslide, Taiwan, based on Saint Venant equations over general topography, Engineering Geology (2008), doi:10.1016/j.enggeo.2008.10.003

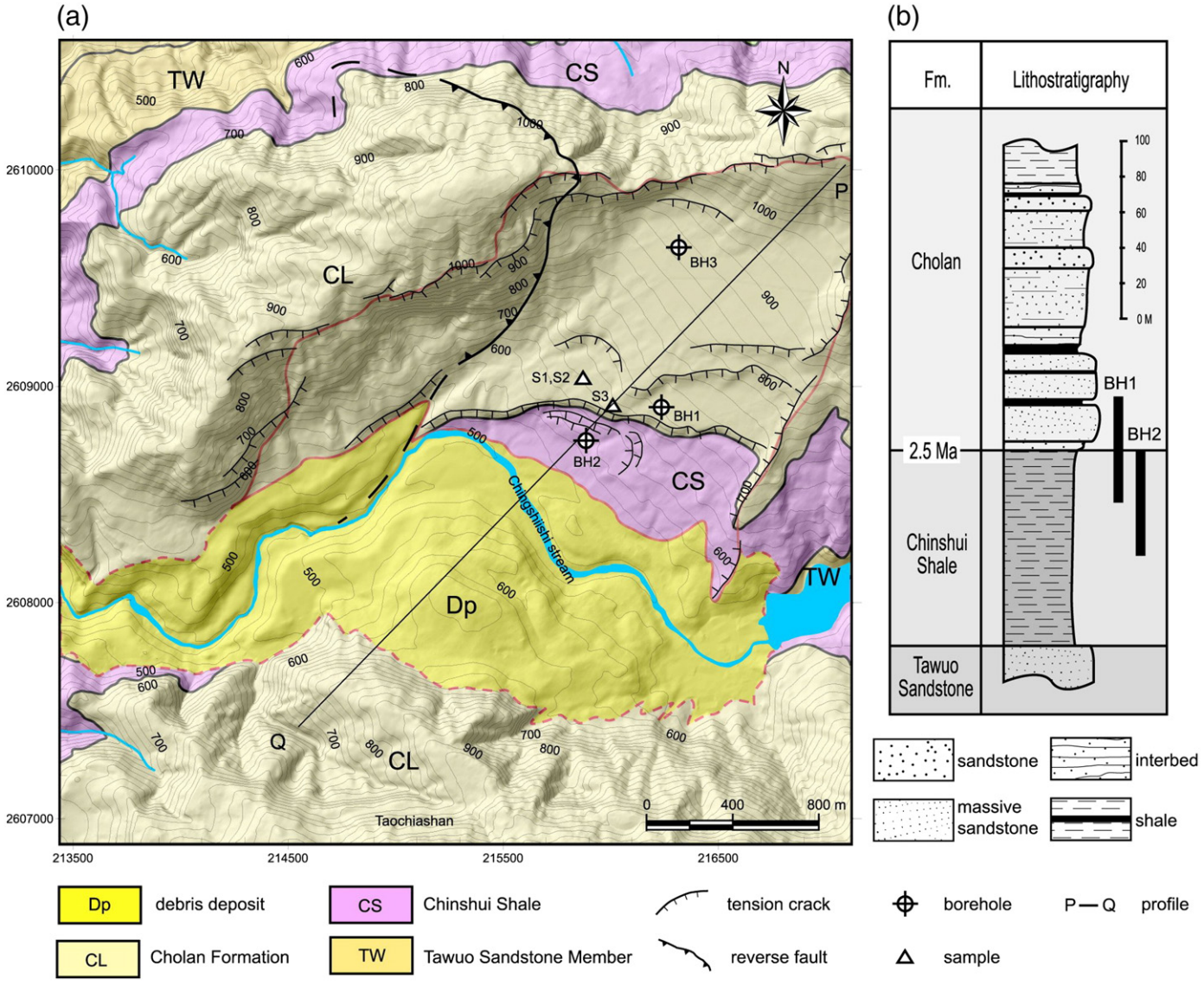

Fig. 2. (a) Geological map and (b) representative stratigraphic section of the study area. Shaded relief map of the Tsaoling region, with 25 m contour interval by the airborne-photo derived DEM, 2000. S1, S2, S3 and BH1, BH2, BH3 are the sampling locations and bore-holes reported by Hung et al. (2002), prior to the earthquake.

level. The usual representative profile for the landslides is along the line $\overline{PQ}$, sketched in the figure. Near the profile, there are material sampling positions, S1, S2, S3 and the investigated bore-holes, BH1, BH2, BH3, of Hung et al. (1994) and Hung et al. (2002), which are also marked. Photographs, Fig. 3, present the visual overview of the area and the result of the landslide.

The geological condition of Tsaoling makes it susceptible to earthquakes and heavy rainfalls. There were landslide events recorded since 1862 and details of each event have been documented in Huang et al. (1983, 2002), Chen et al. (2003, 2006b) and the references therein. This is because the morphology of the area is dominated by sedimentary rocks that dip in the same direction as the slope, 14° on

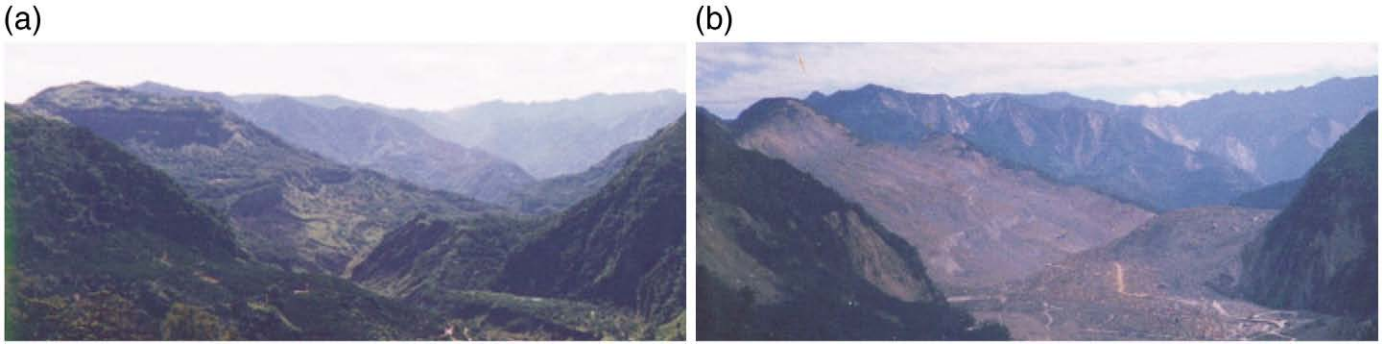

Fig. 3. Overview of the Tsaoling landslide, looking from west to east. (a) Photograph taken before 1999 Chi-Chi earthquake. (b) Photograph taken from the same view point after the earthquake.

Please cite this article as: Kuo, C.Y., et al., Simulation of Tsaoling landslide, Taiwan, based on Saint Venant equations over general topography, Engineering Geology (2008), doi:10.1016/j.enggeo.2008.10.003

average. The profiles, Fig. 4, along $\overline{PQ}$ depict the change of topography by the 1941, 1979 and the 1999 landslides. They also present the two major geological surface layers: the Cholan formation and the Chinshui shale below. A typical geological stratigraphic profile is shown in Fig. 2(b).

The Cholan formation consists mainly of fine-grained sandstones and inter-calated shales. This layer constitutes most of the landslide mass. It has a loose structure with high permeability. On the other hand, the Chinshui shale, on average over 110 m thick, consists of massive mudstone and shale, which has low permeability and loses strength significantly when the water content is high. Extensive material tests have been performed (Hung et al., 2002; Chen et al., 2003, and references therein), but variations among the tests have been found due to the highly irregular natural materials. One of the representative reports is exerted in Table 1. Underneath these layers is the bedrock Tawuo Sandstone formation, which is over 1100 m thick.

There are several weak interfaces in the two layers. They are first the interface between the Cholan formation and the Chinshui shale and the second is the intercalated shales within the Cholan formation. Landslides before 1979 (incl.) all happened due to slip at the interface between the two layers because of the low strength of Chinshui shale. The shale layer is hence exposed to the surface, Fig. 2(a) and formed the 1979 scarp. The scarp is between elevation 650 and 700 m in elevation.

On the contrary, the landslide in 1999 is the first one for which the rock ruptures in the Cholan layer. Field investigation reveals that the failure takes place in the weak thin shale layer in Cholan formation (Chigira et al., 2003). This echoes the weak material strength of the intercalated shale, Table 1. At the detachment surface, numerous brittle features were found. Most fractures, especially open fissures, are approximately perpendicular to bedding planes and reflect the tensile failure. There are localized pseudotachylyte spots found on the sliding surfaces and this indicates that the rock melting processes take place due to friction of the materials (Lin et al., 2001a).

The high saturation indicates the existence of ground-water in the formation. Hung et al. (1994) estimate the ground-water level,

Table 1
Material properties at the sampling positions (Hung et al., 2002)

	CL shale (S1)	CL sandstone (S2)	CS (S3)
Specific weight	2.66	2.68	2.66
Water content	4.0%	2.5%	2.2%
Void ratio	12.79%	12.38%	5.64%
Saturation	72.03%	47.47%	96.84%
Peak friction angle ϕp	20.5	75.3	34.1
Residue friction angle ϕr	21.5	38.8	34.1
Peak cohesion C_p (kPa)	152	272	524
Residue cohesion C_r (kPa)	75	109	71
Slake durability index Id_2	4.8%	67.5%	69.8%
Durability classification[a]	Very low	Medium	Medium
Plastic limit %	17%	NP	NP

CL: Cholan formation, CS: Chinshui shale, NP: Nonplastic.
[a] According to Brown (1981).

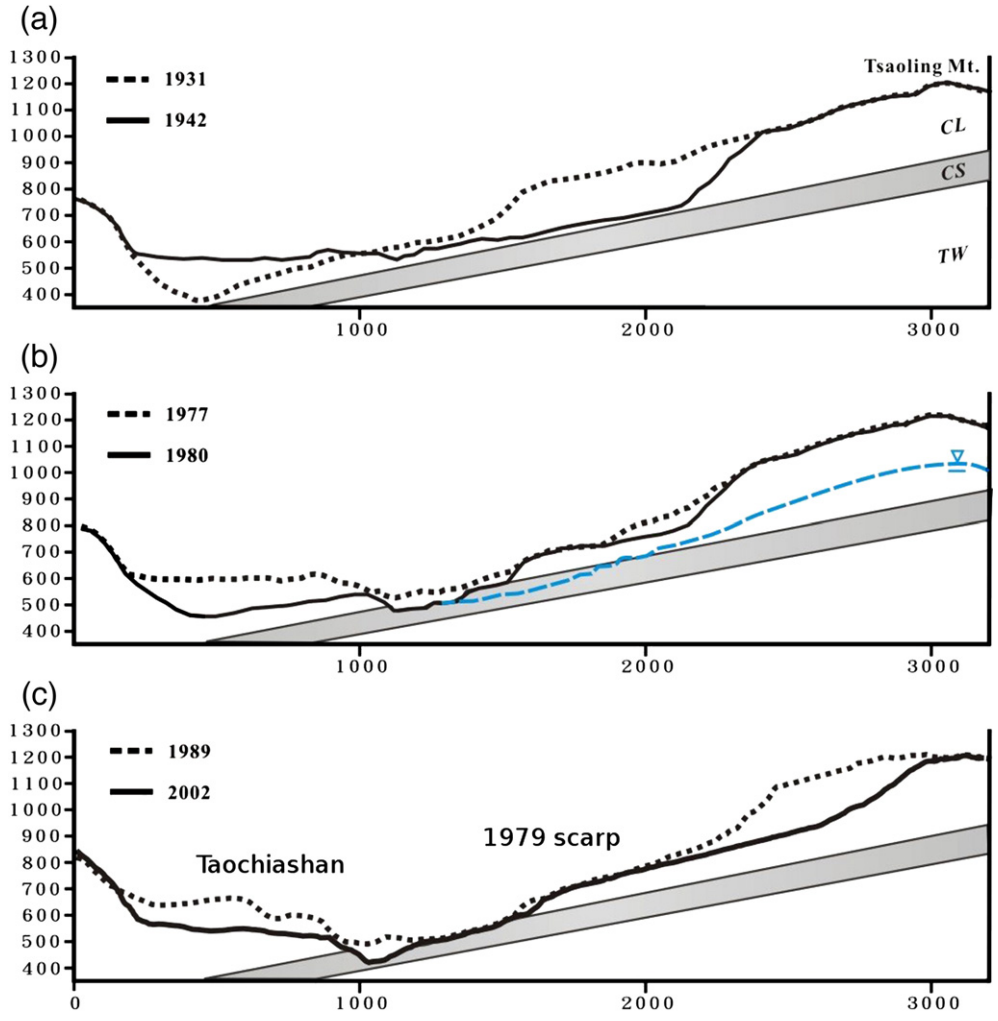

Fig. 4. Reconstructed cross-section of the Tsaoling landslide. (a) Topography change after the 1941 event. (b) After 1979 event and (c) the 1999 landslide (by the Chi-Chi earthquake). Also in (b) the estimated ground-water table (Hung et al., 1994) and (c) the 1979 scarp and the deposit, now called Taochiashan.

Please cite this article as: Kuo, C.Y., et al., Simulation of Tsaoling landslide, Taiwan, based on Saint Venant equations over general topography, Engineering Geology (2008), doi:10.1016/j.enggeo.2008.10.003

sketched in Fig. 4(b). This is based on the findings that constant water outflow is observed from the 1979 scarp interface and rock joints and the water content from samples of the three site bore-holes. The close incidence of the water level and the landslide basal interface strongly indicates the correlation between the strength yield of submerged shale and the earthquake movement. The remaining section of the Cholan layer after the Chi-Chi earthquake along the main profile is still estimated about 100 m and its volume is about 0.27 km^3. This mass is still vulnerable to future hazard events according to the risk analysis by Huang et al. (1983).

3. Formulation

To simulate the landslide motion, detailed composition of the geological materials has yet to be neglected. In addition, the initiation mechanisms are also neglected. These include the failure of the interface under the earthquake motion, rock rupture, and volume dilation of the mass. We assume the process takes place in a relatively short time (compared to the total duration) after the landslide is triggered.

The hydraulic model, SHALTOP^{2D}, utilizes a set of general coordinates that is constructed in a terrain-following way. The topographical coordinates, (ξ,η,ζ), and the fixed reference Cartesian coordinates (x,y,z) are shown in Fig. 5. The topography surface is fixed and described by $z=b(x,y)$ and its normal unit vector is given by

$$\vec{n} = \left(-\frac{\nabla_x b}{\sqrt{1+|\nabla_x b|^2}}, \frac{1}{\sqrt{1+|\nabla_x b|^2}} \right) = (-\mathbf{s}, c) \in \mathbb{R}^2 \times \mathbb{R}^1, \tag{1}$$

where $\nabla_x = e_x \frac{\partial}{\partial x} + e_y \frac{\partial}{\partial y}$ is an $\mathbb{R}^2$ gradient operator. The normal unit vector is decomposed in the way that c is the cosine of $\vec{n}$ and the vertical direction, and $-\mathbf{s}$ is its horizontal projection. The surface curvature tensor of the topography is

$$\mathcal{H} = c^3 \begin{pmatrix} \frac{\partial^2 b}{\partial x^2} & \frac{\partial^2 b}{\partial x \partial y} \\ \frac{\partial^2 b}{\partial x \partial y} & \frac{\partial^2 b}{\partial y^2} \end{pmatrix}, \tag{2}$$

and its components can be explicitly written in terms of c and $\mathbf{s}$, see Bouchut and Westdickenberg (2004).

For simplicity, the avalanche flows only consist of a single phase constituent. Their typical flow depth, H, is usually much smaller than the characteristic length, L. Hence, we have a small scaling parameter ϵ, such that $\epsilon = H/L \ll 1$. The topographical curvature is assumed small, of $O(\epsilon)$. The basal friction is given by the Coulomb friction law, with a friction coefficient, $\mu = \tan\phi$ where ϕ is the friction angle. The magnitude of the friction coefficient is also assumed of $O(\epsilon)$. Under such circumstances, the scaling analysis reveals that the acceleration normal to the topography is negligible and the depth-integration can be carried out by prescribing a velocity profile.

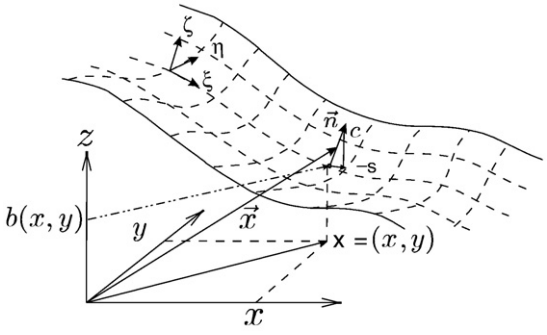

Fig. 5. The coordinate systems.

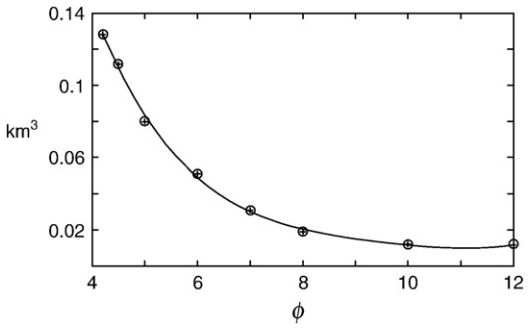

Fig. 6. Accumulated outflow volume versus the basal friction angle.

In the thin flow layer, we assume the flow has a uniform velocity profile across the flow depth h. The three-dimensional velocity, $\vec{u}$, expressed by a so-called velocity parametrization $\mathbf{u} \in \mathbb{R}^2$, such that $\vec{u} = (c\mathbf{u}, \mathbf{s}\cdot\mathbf{u})$. Mathematically, $c\mathbf{u}$ is the tangential components of the contravariant velocity in the terrain-following coordinates. If the basal surface is one-dimensional, $\mathbf{u}$ reduces to one component and its magnitude is equal to the flow speed parallel to the surface. After depth-integration, the governing equations of Saint Venant type read

$$\begin{aligned} &\partial_t h + c\nabla_x \cdot (h\mathbf{u}) = 0, \\ &\partial_t (h\mathbf{u}) + c\nabla_x \cdot (h\mathbf{u} \otimes \mathbf{u}) = -\frac{h}{c}(\mathbf{I} - \mathbf{s} \otimes \mathbf{s})\nabla_x (g(hc+b)) - \frac{h}{c}(\mathbf{u}^t \mathcal{H} \mathbf{u})\mathbf{s} \\ &\qquad + \frac{h}{c}(\mathbf{s}^t \mathcal{H} \mathbf{u})\mathbf{u} - \frac{g\mu ch\mathbf{u}}{\sqrt{c^2|\mathbf{u}|^2 + (\mathbf{s}\cdot\mathbf{u})^2}} \left(1 + \frac{\mathbf{u}^t H \mathbf{u}}{gc}\right). \end{aligned} \tag{3}$$

The first term on the right hand side is the gradient of the hydraulic pressure and the gravity force. The second and third terms are the sources due to the topographical curvature, i.e. Christoffel symbol effects, where the former has the form of the centrifugal force of the flow and the latter arises due to the particular choice of the velocity parametrization. The last term is the basal Coulomb friction force. In addition, it is interesting to notice that the gradient operator is defined in the Cartesian coordinates so that it suits the incorporation with geological metrics. This is in contrast with the models proposed by Savage and Hutter (1989, 1991), Gray et al. (1999) and Wieland et al. (1999), where the model equations are defined in the terrain-fitted curvilinear coordinates.

The resulting system of governing equations is of hyperbolic type. Equations of this type allow the formation of discontinuities and weak solutions (shocks). The model equations are numerically solved by a shock capturing finite volume scheme based on Suliciu's approximate Riemann solver. Source terms are treated efficiently by employing a well-balancing technique, which ensures the property of preserving steady states at the discrete level. For a detailed description of the implementation of the numerical scheme, we refer to Mangeney-Castelnau et al. (2005), Bouchut (2004), and Mangeney et al. (2007).

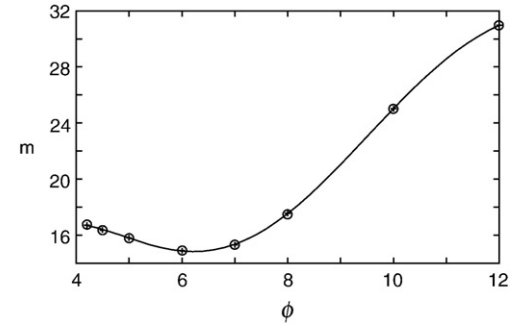

Fig. 7. Standard deviation of deposit depth versus the basal friction angle.

Please cite this article as: Kuo, C.Y., et al., Simulation of Tsaoling landslide, Taiwan, based on Saint Venant equations over general topography, Engineering Geology (2008), doi:10.1016/j.enggeo.2008.10.003

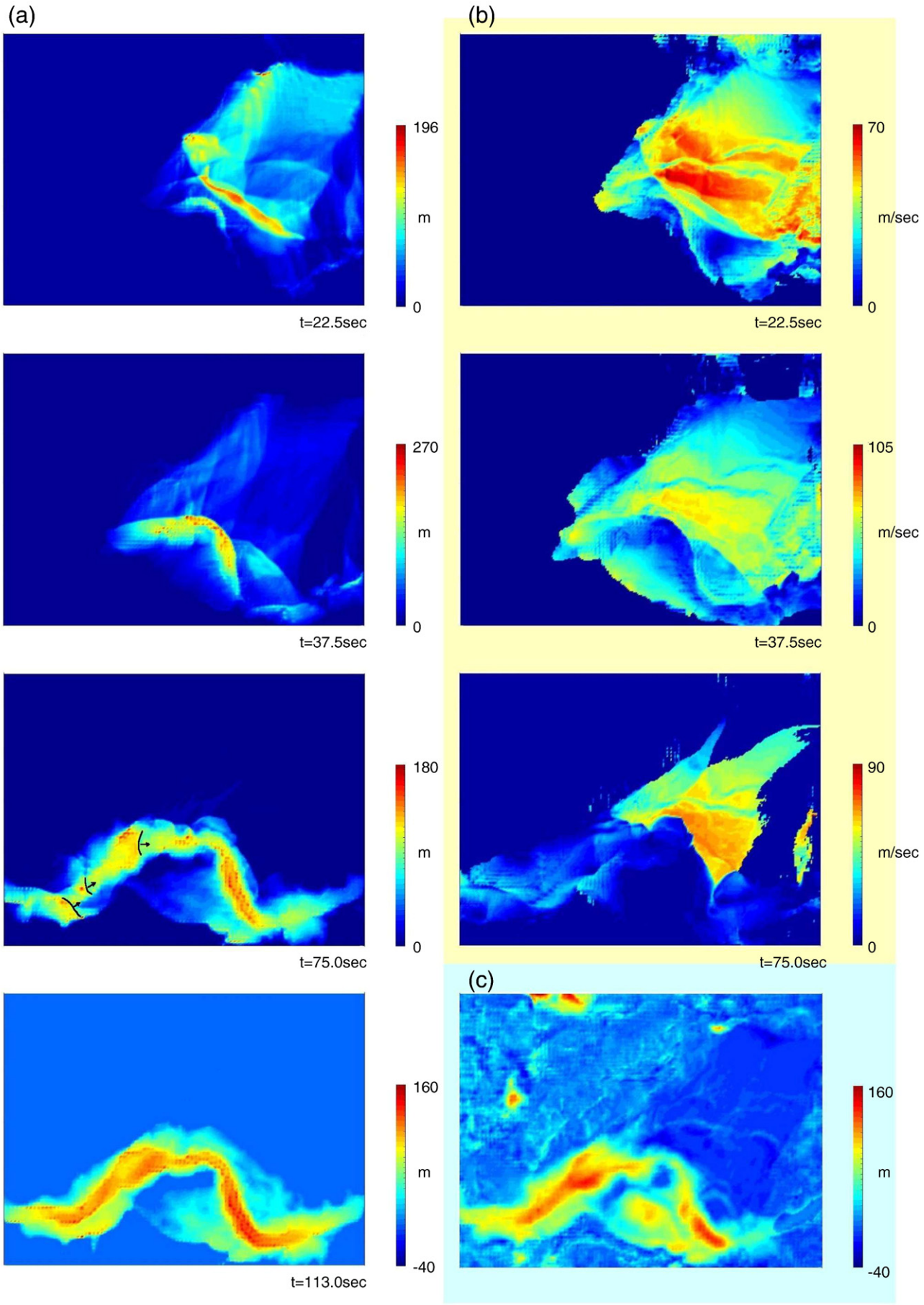

Fig. 8. Simulation snapshots. (a) Flow depths normal to the basal topography, (b) velocity and (c) measurement in 2000.

Please cite this article as: Kuo, C.Y., et al., Simulation of Tsaoling landslide, Taiwan, based on Saint Venant equations over general topography, Engineering Geology (2008), doi:10.1016/j.enggeo.2008.10.003

4. Result and discussion

In Taiwan, aerial photograph interpretation and mapping are routinely performed by the Agricultural and Forestry Aerial Survey Institute of Taiwan. For the present geomorphological study associated with the 1999 Tsaoling landslide, we take the 1989 and 2000 digital elevation models (DEM). They are based on the aerial photos with ground measurement corrections and have mesh resolutions 40×40 m and 10×10 m respectively. Comparing the different sets of data, we estimate the landslide-related mass transfer and basal topography in the numerical model.

To cover the landslide area, a computation domain of 3692×2795 m is setup and discretized into 284×215 rectangular cells. Each grid cell has a size 13×13 m. To enhance the numerical stability, we set a cut-off depth of 1 cm. The maximum time for the simulation is set to 150 s and, in all the calculation cases, mass movements come to rest within about 2 min. No flux conditions are applied on the north and south boundaries (of the computation domain). Outgoing conditions, instead, are used on the east and west borders to account for the outgoing flows from the river valley and, partly, from the dip slope.

Because the model cannot cope with volume dilation at initiation, we increase the initial scar depth by a linear factor, determined from comparing the final deposit volume, up to ±3%, with the real measurement. The factor ranges from 1.1 to 1.7 as the basal friction angle varies from 12° to 4.5°. The increase of the factor comes with the increase of outflow from the computation domain for the small friction cases, Fig. 6. Landslide deposit outside the current investigated area is observed in the field, especially the right side outside the calculation boundary, though the small amount is not taken into account.

The best fit of the basal friction is evaluated by minimizing the root mean square (rms) of the depth difference between the simulation and the real data over the Chinshui deposit valley. The rms error versus the prescribed friction angle is sketched in Fig. 7. The angle corresponding to the minimum error is about 6°. This is considerably lower, 72%, than the internal peak friction angle of the Cholan formation shale. The initial volume factor is 1.36. The slightly higher factor than the usual 20–25% accounts for the simulation outflow. The standard deviation of the deposit height is 15 m and the accumulated outflow volume is about 0.05 km^3 under this basal friction angle.

This basal friction angle lowering phenomenon can be partly explained by the collective behavior of granular flows, Tai and Lin (in press). Based on the DEM simulation, Campbell et al. (1995) show a negative correlation between the apparent basal friction and the flow volume by fixing the discrete particle size uniformly at 1 m in diameter. Another important factor is the water pore-pressure effect. Fluidization of the debris flow by pore water pressure has been shown to be an important factor (Goguel, 1978; Legros, 2002) and has been treated as a solid volume factor on the basal Coulomb friction (Iverson and Denlinger, 2001). In the field, the existence of the water content is backed by the fact that fresh water seepages from the interfaces between the geological formations and joints, Chen et al. (2003). However, this effect is not modeled by the current shallow flow theory. An indirect verification of the water effects can be seen from the analysis based on DEM for Jiufengershan landslide (Chang et al., 2005). With these two influencing factors in mind, our fitted friction angle is in a reasonable range, e.g. the estimation in Fig. 5 (Legros, 2002).

Fig. 8(a) and (b) shows the sequence of transient flow depths and speeds of the debris flow motion. For clarity, the flow is set zero outside the main landslide area. Two curved flow fronts are observed shortly after initiation, e.g. t=22.5 s, Fig. 8$(a)_1$. Formation of the two flow fronts is because the initial avalanche mass composes a thin layer extending forefront of the main bulk, e.g. Fig. 4(a). This leads to a flow with two different depth scales.

The maximum speed reaches about 75 m/sec when the main debris volume flows across the 1979 scarp upon entering the river valley, Fig. 8(b). At such speed, the simulation confirms the field observation that the landslide is of rock avalanche type, according to the classification by Cruden and Varnes (1996) and Hungr et al. (2001). By this momentum, the flow further crosses Chinshui river at about half minute after initiation and deposits at the opposite of the river band. The flow is also diverted and spread into the river channel. This is in contrast to the DEM simulation (Tang and Hu, 2004), where the authors minimize the internal friction angle to almost zero to observe this phenomenon.

Upon the flow enters the river channel, it interacts with the surrounding topography and the channel banks. This forms complicated flow patterns, notably the three dimensional surge structures. For example, Fig. 8$(a)_3$, we can see the reflected surges traveling upstream to where the debris originates. The depth jumps across the surge front are about of the order of 10 m and propagate in the sketched directions.

Dramatic flow interactions can be seen from the transient sequence of the main $\overline{PQ}$ profile, Fig. 9. The two major flow fronts are seen in the profile at t=18 s. Around t=36 s, the main flow reaches the river valley. The second front quickly catches up with the first when it is decelerated by the river bed. An upstream traveling shock, with a magnitude over 100 m, is finally formed upon the flow impinging on the opposite bank of the river channel. While the shock propagates slowly upstream (from t=36 to 90 s), the flow is continuously fed into the deposit region and forms a secondary surge front. Both surges are

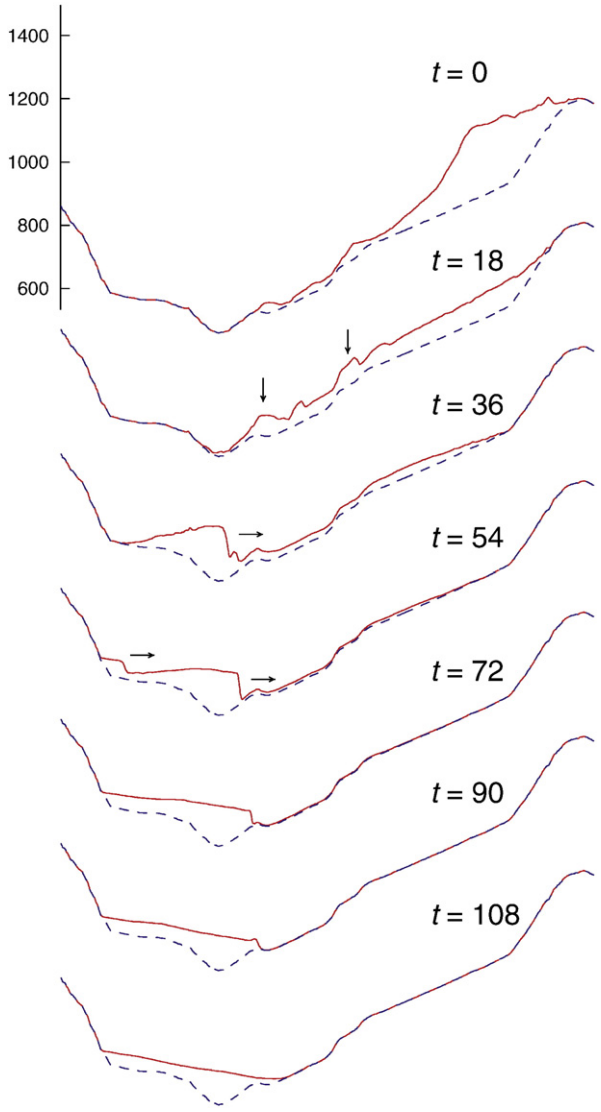

Fig. 9. Waterfall plot of the landslide sequence on the profile.

Please cite this article as: Kuo, C.Y., et al., Simulation of Tsaoling landslide, Taiwan, based on Saint Venant equations over general topography, Engineering Geology (2008), doi:10.1016/j.enggeo.2008.10.003

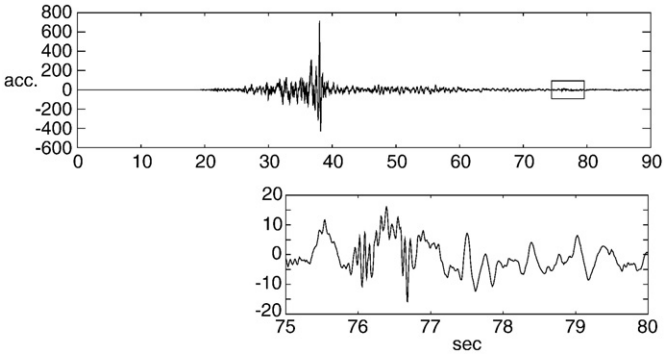

Fig. 10. Vertical ground acceleration of the earthquake at station CHY080.

then dissipated by the friction force and settled into a profile with a smooth surface.

At $t=113$ s, the flow is almost at rest. The simulated deposit, say Fig. 8(a)$_4$, is compared with the measurements. The thickest deposit occurs at the middle section of the Chinshui river. The depth of the deposit opposite the river, however, is underestimated by the simulation nor the deposit hill, Taochiashan, is seen. This is because the Eulerian constituent does not have the internal friction angle at which the flow reposes. Simulation beyond $t=113$ s shows indistinguishable surface change. Along the river bank, a similar effect of the fluid can be seen and shows that the simulation deposit is more wide-spread than in reality. These discrepancies call for future investigations with different material constitutive laws.

It is also of interest whether such a landslide induces ground movement which is ever recorded in the nearby strong-earthquake station. Due to high seismic activity of this island, Taiwan has the densest earthquake monitoring network in the world (Tsai and Lee, 2005). The nearest station, CHY080, is less than 0.5 km northwest to the landslide site boundary. The recording of the vertical acceleration is shown in Fig. 10, where the time origin is offset to the earthquake time at the epicenter. It is argued that the instance marked in the figure shows a unique characteristic, that is the burst of the high frequency components at $t=75.8$ s for about one second or so. These signals are not known to be associated with aftershocks and neither appear in records of other stations nearby. The time span to the main earthquake signal peak is about 38 s. It is suggested by the coincidence of the time span that the signals may be somewhat correlated to the impact of the flow to the river valley. On this conjecture, preliminary investigations have been initiated.

5. Conclusion and future respects

From the simulation results, we conclude that the landslide roughly takes 2 min, which somewhat agrees with the estimation of local survivors. The best fit of the basal friction angle is 6°. At this angle, the initial volume factor is about 1.36 and about 24% of the total debris volume leaves the calculation domain from the river valley. Since the material strength, especially the slake durability index, is weak in the thin shale layer of Cholan formation, it is subjected to a loss of strength when it is weathered in the ground-water table and ruptured during the earthquake. The friction angle further reduces when the mass movement is initiated. The maximum landslide velocity reaches about 75 m/s, which occurs in the region between the 1979 scarp and the river bank. Generally, good agreements are found in both the height and spread area of the deposit comparing the simulation and field measurements, at an rms error 15 m compared to the maximum deposit depth about 140 m. The major discrepancies are seen from that the simulation deposit is more wide-spread in the river channel and the thinner deposit on the opposite river bank, which, in reality, forms a small deposit hill.

The present simulation is performed in the frame of Eulerian fluids with a basal friction. This is shown to be the major constituent in the hierarchy of isotropic incompressible fluid avalanche models, Luca et al. (in press). A parameter study using a sole basal friction angle is performed and this constant angle is applied for the whole flow. This aggressive simplification allows minimizing the number of influencing parameters so as to focus on the applicability of the current model with a complicated real topography.

However, discrepancies from comparing with the real measurements are also found that urge future investigations of the landslide with more sophisticated constitutive laws. Different friction laws have been proposed. For example, Pouliquen and Forterre (2002) postulate a universal scaling law of the flow velocity on the surface inclination angle, roughness, and flow depth. On this law, the phenomena of self-channeling and levée formation of granular flow are verified (Mangeney et al., 2007) and simulations of real landslides based on this flow law also give reasonable results (Pirulli and Mangeney, 2008). This could be interesting to test for the Tsaoling landslide. The other alternative to be examined is a material constituent of Mohr–Coulomb type. This has been widely applied in various geofluid models and its anisotropic property has been categorized in a special hierarchy of avalanche models where the stresses acting on planes perpendicular to the basal surface are no longer negligible (Luca et al., in press). It is also shown therein that the anisotropic stress state can be uniquely determined from the principal axes of the local strain state without the need of ad hoc assumptions.

Former risk analyzes, Huang et al. (1983, 2002), and Chen et al. (2003), constantly raise alerts on possible future landslides, for example, the portion of Cholan formation near Tsaoling Mountain. Deducing the mass volume that was released in the Chi-Chi earthquake, there is still about 0.27 km^3 unstable material resting at its current position, based on a pessimistic estimation by Huang et al. (1983). While advanced theoretical models are still being pursued, the current model has shown to have capabilities to provide informative estimation of the influence area of potential future landslide events for hazard prevention purposes.

Acknowledgments

The authors thank Prof. K. Hutter for his efforts for initiating this collaborating research and discussion with Dr. I. Luca. The work is supported in part under grant NSC-97-2221-E-260-018-, NSC, Taiwan, ROC.

References

Bouchut, F., 2004. Nonlinear Stability of Finite Volume Methods for Hyperbolic Conservation Laws and Well-balanced Schemes for Sources. Birkhauser Verlag.
Bouchut, F., Westdickenberg, M., 2004. Gravity driven shallow water models for arbitrary topography. Comm. Math. Sci 2, 359–389.
Brown, E.T. (Ed.), 1981. Rock Characterization, Testing and Monitoring: International Society of Rock Mechanics Suggested Method. Pergamon Press, Oxford.
Campbell, C.S., Cleary, P.W., Hopkins, M., 1995. Large-scale landslide simulations: global deformation, velocities and basal friction. J. Geophys. Res. 100, 8267–8273.
Chang, K.J., Taboada, A., Lin, M.L., Chen, R.F., 2005. Analysis of landslide by earthquake shaking using a block-on-slope thermo-mechanical model: example of Jiufengershan landslide, central Taiwan. Eng. Geol. 80, 151–163.
Chen, T.C., Lin, M.L., Hung, J.J., 2003. Pseudostatic analysis of Tsao-ling rockslide caused by Chi-Chi earthquake. Eng. Geol. 71, 31–47.
Chen, H., Crosta, G.B., Lee, C.F., 2006a. Erosional effects on runout of fast landslides, debris flows and avalanches: a numerical investigation. Géotech. 56, 305–322.
Chen, R.F., Chang, K.J., Angelier, J., Chan, Y.C., Deffontaines, B., Lee, C.T., Lin, M.L., 2006b. Topographical changes revealed by high-resolution airborne lidar data: the 1999 Tsaoling landslide induced by the Chi-Chi earthquake. Eng. Geol. 88, 160–172.
Chen, R.F., Chan, Y.C., Angelier, J., Hu, J.C., Huang, C., Chang, K.J., Shih, T.Y., 2005. Large earthquake-triggered landslides and mountain belt erosion: the Tsaoling case, Taiwan. C. R. Geoscience 337, 1164–1172.
Chigira, M., Wang, W.N., Furuya, T., Kamai, T., 2003. Geological causes and geomorphological precursors of the Tsaoling landslide triggered by the 1999 Chi-Chi earthquake, Taiwan. Eng. Geol. 68, 259–273.
Cruden, D.M., Varnes, D.J., 1996. Landslide types and processes. In: Turner, A.K., Schuster, R.L. (Eds.), Landslide Investigation and Mitigation. Transp. Res. Board, vol. Special Rep. 247. US National Res. Council, Washington, DC., pp. 36–75. Ch. 3.
Denlinger, R.P., Iverson, R.M., 2001. Flow of variably fluidized granular masses across three-dimensional terrain. 2. Numerical predictions and experimental tests. J. Geophys. Res. 106, 553–566.

Goguel, J., 1978. Scale-dependent rockslide mechanisms, with emphasis on the role of pore fluid vaporization. In: Voight, B. (Ed.), Rockslides and Avalanches, 1. Natural phenomena. Elsevier, Amsterdam, pp. 693–705.
Gray, J.M.N.T., Wieland, M., Hutter, K., 1999. Gravity-driven free surface flow of granular avalanches over complex basal topography. Proc. R. Soc. A A455, 1841–1874.
Gray, J., Tai, Y.-C., Noelle, S., 2003. Shock waves, dead-zones and particle-free regions in rapid granular free surface flows. J. Fluid Mech 491, 161–181.
Huang, C.S., Ho, H.C., Liu, H.C., 1983. The geology and landslide of Tsaoling area, Yun-Lin, Taiwan (in Chinese). Bulletin of the Central Geological Survey 2, 95–112.
Hung, J.J., 2000. Chi-Chi earthquake induced landslides in Taiwan. Earthq. Eng. Eng. Seismol. 2, 25–33.
Hung, J.J., Lee, C.T., Lin, M.L., 2002. Tsao-ling rockslides, Taiwan. In: Evans, S.G., DeGraff, J.V. (Eds.), Catastrophic Landslides: Effects, Occurrence, and Mechanisms. Geo. Soc. Am. Rev. Eng. Geo., vol. 15. Boulder, Colorado, pp. 91–115.
Hung, J.J., Lin, M.L., Lee, C.T., 1994. A stability analysis of the Tsao-ling landslide area. In: '94 Rock Engineering Symposium in Taiwan. Chung-Li, Taiwan, pp. 459–467, (in Chinese).
Hungr, O., Evans, S.G., Bovis, M., Hutchinson, J.N., 2001. Review of the classification of landslides of the flow type. Environ. Eng. Geosci. 7, 221–238.
Iverson, R.M., Denlinger, R.P., 2001. Flow of variably fluidized granular masses across three-dimensional terrain. 1. Coulomb mixture theory. J. Geophys. Res. 106, 537–552.
Legros, F., 2002. The mobility of long-runout landslides. Eng. Geol 63, 301–331.
Liao, H.W., 2000. Landslides triggered by Chi-Chi earthquake. Master's thesis, National Central Univ., Chungli (in Chinese).
Lin, A., Chen, A., Liau, C.F., Lee, C.T., Lin, C.C., Lin, P.S., Wen, S.C., Ouchi, T., 2001a. Frictional fusion due to coseismic landsliding during the 1999 Chi-Chi (Taiwan) m_l 7.3 earthquake. Geo. Res. Lett. 28, 4011–4014.
Lin, A., Ouchi, T., Chen, A., Maruyama, T., 2001b. Co-seismic displacements, folding and shortening structures along the Chelungpu surface rupture zone occurred during the 1999 Chi-Chi (Taiwan) earthquake. Tectonophysics 330, 225–244.
Luca, I., Hutter, K., Tai, Y.C., Kuo, C.Y., in press. A hierarchy of avalanche models on arbitrary topography. ACTA Mech.
Lucas, A., Mangeney, A., 2007. Mobility and topographic effects for large valles marineris landslides on mars. Geo. Res. Lett. 34, L10201.
Mangeney-Castelnau, A., Bouchut, F., Vilotte, J.P., Lajeunesse, E., amd M. Pirulli, A.A., 2005. On the use of Saint Venant equations to simulate the spreading of a granular mass. J. Geophys. Res. 110, B09103.
Mangeney, A., Bouchut, F., Thomas, N., Vilotte, J.P., Bristeau, M.O., 2007. Numerical modeling of self-channeling granular flows and of their levee-channel deposits. J. Geophys. Res. 112, F02017.
McDougall, S., Hungr, O., 2004. A model for the analysis of rapid landslide motion across three-dimensional terrain. Can. Geotech. J. 41, 1084–1097.
Pirulli, M., Mangeney, A., 2008. Results of back-analysis of the propagation of rock avalanches as a function of the assumed rheology. Rock Mech. Rock Eng. 41, 59–84.
Pouliquen, O., Forterre, Y., 2002. Friction law for dense granular flows: application to the motion of a mass down a rough inclined plane. J. Fluid Mech. 453, 133–151.
Pudasaini, S.P., Hutter, K., 2003. Rapid shear flows of dry granular masses down curved and twisted channels. J. Fluid Mech. 495, 193–208.
Pudasaini, S.P., Hutter, K., 2007. Avalanche dynamics, dynamics of rapid flows of dense granular avalanches. Springer.
Savage, S.B., Hutter, K., 1989. The motion of a finite mass of granular material down a rough incline. J. Fluid Mech. 199, 177–215.
Savage, S.B., Hutter, K., 1991. The dynamics of granular material from initiation to runout. Part I: analysis. Acta Mech. 86, 201–223.
Tai, Y.C., Lin, Y.C., in press. A focused view of the behavior of granular flows down a confined inclined chute into the horizontal run-out zone. Phys. Fluid.
Tang, C., Hu, J., 2004. 3-d numerical investigation of the Tsaoling landslide induced by Chi-Chi earthquake, Taiwan. Eos Trans. AGU Fall Meet. Suppl, vol. 85. AGU, pp. S11A–1008.
Tsai, Y.B., Lee, C.P., 2005. Strong motion instrumentation programs in Taiwan. NATO Science Series, vol. 58. Springer, Netherlands, pp. 255–278.
Wieland, M., Gray, J.M.N.T., Hutter, K., 1999. Channelized free-surface flow of cohesionless granular avalanches in a chute with shallow lateral curvature. J. Fluid Mech. 73–100.

Please cite this article as: Kuo, C.Y., et al., Simulation of Tsaoling landslide, Taiwan, based on Saint Venant equations over general topography, Engineering Geology (2008), doi:10.1016/j.enggeo.2008.10.003